Proceedings of ASME Turbo Expo 2011
GT2011
June 6-10, 2011, Vancouver, British Columbia, Canada

GT2011-46373

Effects of Endwall Motion on the Aero-Thermal Performance of a Winglet Tip in a HP Turbine

Chao Zhou*
State Key Laboratory for Turbulence and Complex Systems, College of Engineering, Peking University, Beijing, China

Howard Hodson
Whittle Laboratory
Department of Engineering, University of Cambridge, UK

Ian Tibbott and Mark Stokes
Rolls-Royce plc, Derby
UK

ABSTRACT

In a gas turbine, the casing endwall moves relative to the blades. In this paper, numerical methods are first validated using experimental results for a stationary endwall. They are then used to study the effects of endwall motion on the aero-thermal performance of both winglet tips with and without tip film cooling at a tip gap of 1.9%C.

The endwall motion imposes a tangential force on the flow. A scraping vortex is formed and the flow pattern within the tip gap, changes significantly. The tip leakage mass flow rate that exits the tip gap from the suction side edge reduces by about 42% with endwall motion. Overall, the endwall motion reduces the tip leakage loss by 15%. The flow field downstream of the cascade also changes with endwall motion.

With endwall motion, the changed flow pattern within the tip gap significantly changes the distribution of the Nusselt number on the winglet tip. For the winglet tip without tip film cooling, the Nusselt number and the heat load decrease with endwall motion. This is mainly due to the reduction in the tip leakage mass flow ratio, which reduces the leakage velocity over the tip.

On the winglet tip with tip film cooling, the cooling effectiveness increases by 9% with endwall motion. Combined with the reduced Nusselt number, the heat flux on the winglet tip with tip film cooling reduces by 31% with endwall motion. The cooling effectiveness on the near tip region of the pressure side remains almost unchanged, but the heat flux rate in this area reduces. This is because the reduced tip leakage mass flow ratio reduces the Nusselt number. With the moving endwall, the thermal performance of the suction side surface of the blade is affected by the scraping vortex. The effects of endwall motion should be considered during the design of the blade tip.

INTRODUCTION

In unshrouded high pressure axial turbines, the tip leakage flow results in an undesirable loss of efficiency. It can also result in excessively high metal temperatures on the blade tip. Obtaining a good aero-thermal performance of the blade tip represents a major challenge for turbine designers.

The driving pressure difference of the tip leakage flow is approximately that between the static pressure on the pressure side at blade midspan and the static pressure at the suction side exit of the tip gap (Rains [1]). By using winglets on the blade tip, the driving pressure difference of the tip leakage flow decreases. This reduces the tip leakage mass flow rate. The blade surface normal static pressure gradient is generally much higher near the blade suction side than that near the blade pressure side. Therefore, a winglet of the same size on the suction side of the blade tip achieves a greater reduction in the driving pressure difference than a winglet on the pressure side of the tip. (Schabowski and Hodson [2])

Winglet tips were found to be able to reduce the tip leakage loss by Schabowski and Hodson [2] in a cascade and by Liu et al. [3] using a low aspect ratio turbine. In a cold flow high speed engine rig, Harvey et al. [4] found that the winglet tip performed as well as a shrouded tip with two fins in terms of reducing the tip leakage loss (45% less than a flat tip).

However, an improvement in the aerodynamic efficiency when using winglet tips was not always observed in rotating rigs. A turbine test reported by Harvey [5] showed that the winglet tips provided no improvement in stage efficiency. It was concluded that if these winglet tips did reduce the tip leakage flow over the tip, then it must have been at the expense of increased losses in the passage flow due to the use of the winglet.

Cooling air is often used to improve the life of the tips in high pressure turbines. Tip coolant injection was observed to be able to partially block the tip leakage flow, by, for example, Zhou and Hodson [6]. Nevertheless, the loss changed only slightly due to the coolant because the increase or decrease of the tip leakage flow due to the coolant injection is small. Hofer and Arts [7] found that with coolant injection, the change of the tip leakage loss is marginal (about ±6%). In a cold flow rotating rig, Rao and Camci [8] found a significant reduction of the stagnation pressure deficit at the exit of the stage when using coolant ejection from the top of a flat tip.

* The work presented in this paper was carried out in the Whittle Laboratory, Cambridge University.
Email:chao.zhou@cantab.net

Quite a few publications report studies of the thermal performance of both flat tips and squealer tips with and without tip film cooling. A review can be found in Bunker [9]. Winglet tips were found to have lower Nusselt numbers by Papa et al. [10] in a low speed cascade. However, in a transonic linear cascade, O'Dowd et al. [11] found that the winglet has a 13% higher average Nusselt number than that of a flat tip. Due to the large surface area of the winglet tip, the heat load of the winglet tip was 2.7 times higher than that of a flat tip. In a cascade, Christophel et al [12] found that the coolant ejected from the dust holes near the tip leading edge of a flat tip effectively cooled the areas around it, especially at a small tip gap. Newton [13] found that the location of the cooling holes is very important to the effectiveness of the cooling air. Cases with coolant injection from both the tip and the pressure side near the tip were studied by Ahn et al. [14] using a flat tip and a cavity tip. In general, the cooling effectiveness increased as the coolant mass flow rate increased.

In an engine, the casing wall moves relative to the blade tips. Generally, the loss mechanisms of the leakage flow with endwall motion are not dissimilar to the cases when the endwall is stationary, e.g. Yaras and Sjolander [15]. Nevertheless, the dragging of the viscous flow by moving endwall has several effects on the aero-thermal performance of tip leakage flow.

Most studies observed a reduction in the tip leakage mass flow rate due to the endwall motion. In a water analogy rig, Graham [16] found that at a small tip clearance of 0.6 percent of the span, the tip leakage flow would be eliminated by increasing the speed of the moving belt, which simulated the relative endwall motion. Yaras and Sjolander [17] found that the passage vortex was enhanced with endwall motion. Using numerical methods, Tallman et al. [18] found that the relative endwall motion strongly enhanced the near casing secondary flow and reduced the tip leakage flow.

The relative endwall motion also affects the tip leakage flow pattern within the tip gap. The size of the separation zone near the pressure side edge of the flat tip reduces due to the endwall motion. This was observed by Yaras and Sjolander [15] using three-hole probe measurements inside the tip gap, by Palafox et al. [19] using PIV measurement and by Krishnababu et al. [20] using numerical methods. McCarter [21] found that the tip leakage vortex appeared closer to the suction side surface of the blade in a cold flow research turbine due to the endwall motion. This was also observed by Tallman et al. [18] and Yang et al. [22].

In terms of the thermal performance, the effect of endwall motion was studied mainly on tips without tip film cooling. Srinivasan and Goldstein [23] found that endwall motion only affected the thermal performance of a flat tip at the smallest tip gap of 0.6%C. In this case, a reduction of 9 percent of the heat/mass transfer in the mid-chord part of the flat tip was obtained. No obvious changes of the heat/mass transfer of the tip was observed at tip gaps larger than 0.86 percent of the chord due to the relative endwall motion. In a rotating cold flow turbine, at a tip gap about 2.5% chord, Rhee and Cho [24] found that the heat/mass transfer of the flat tip was slightly (less than 10%) lower than that of the stationary case. In a large scale linear cascade, Palafox et al. [25] found that the endwall motion altered the locations of the area of high Nusselt numbers due to the change in the location of the flow reattachment. The endwall motion caused a reduction in the average tip Nusselt number of between 7.5% and 13.3% for tip gaps from 0.56% to 1.68% of span.

This paper investigates the effects of the endwall motion on the aero-thermal performance of a winglet tip without and with coolant injection. The objectives of the paper are to understand the effects of the endwall motion on the aerodynamic performance, including the flow pattern over the tip, the flow downstream of the cascade and the tip leakage loss, and to understand the effects of the endwall motion on the thermal performance, including the cooling effectiveness and the heat flux rate.

NOMENCLATURE

C	Blade chord
C_x	Axial chord
C_y	Tangential chord
C_p	Stagnation pressure loss coefficient = $(p_{01}-p)/(p_{01}-p_2)$
$C_{p,0}$	Stagnation pressure loss coefficient = $(p_{01}-p_0)/(p_{01}-p_2)$
F	Viscous shear force
h	Heat transfer coefficient $= q/(T_{aw}-T_w)$
h_{rate}	Heat flux rate $= q/(T_{01}-T_{0w})$
k_{air}	Thermal conductivity of the air
Nu	Nusselt Number $= hC/k_{air}$
p	Static pressure
p_0	Stagnation pressure
q	Local heat flux per unit area
Q	Overall heat flux
Re	Reynolds number $\mathrm{Re} = \rho VC/\mu$
T	Temperature
T_0	Stagnation temperature
T_{aw}	Adiabatic wall temperature
T_w	Wall temperature
U	Relative velocity of the endwall
V	Velocity
V_x	Axial velocity
W	Relative velocity
$\dot{W}$	Work, relative velocity
$Y_{p\text{-}total}$	Total loss coefficient
$Y_{p\text{-}tip}$	Tip leakage loss coefficient
z	Coordinate in blade spanwise direction
η	Cooling Effectiveness $= (T_{aw}-T_{01})/(T_{0c}-T_{01})$
Θ_E	Non-dimensional engine temperature $\Theta_E = (T_{01}-T_{0c})/(T_{01}-T_w)$
ρ	Density
μ	Dynamic viscosity
ϕ	Flow Coefficient $= V_{x,1}/U$

Subscripts

1	Cascade inlet free stream
2	Cascade exit (45%C_x downstream of cascade)
3	Mixed-out exit condition

EXPERIMENTAL METHODS

The experimental studies of the aero-thermal performance of the winglet tip were carried out in a low speed linear cascade with a stationary endwall. The experimental results were used to validate the numerical methods, which were used to study the effects of the endwall motion. As the current research is based on the low speed cascade, the effects associated with compressibility, such as supersonic expansion and shock wave recovery are not studied. Key parameters of the cascade are presented in Table 1.

Fig. 1 shows the overall layout of the cascade. This cascade is comprised of six blades. Two boundary layer bleed slots are located 1.2 axial chords upstream of the blade leading edge on both the hub and the casing endwalls of the cascade. The widths of these boundary layer bleed slots are fixed. Boundary layer bleed slots also exist just upstream of the leading edge of the top and the bottom blade of the cascade. The widths of these two boundary layer bleed slots are adjustable so that they can be used to adjust the periodicity of the cascade. A tailboard is also used at the tailing edge of the top blade to adjust the periodicity of the cascade. Once good periodicity of the cascade was achieved, the width of the bleed slots and the position of the trailing edge tail-board remained unchanged for all of the experiments.

Number of Blades	6
Chord (C)	200mm
Pitch/Chord ratio	0.9
Axial Chord (C_x)	124mm
Aspect Ratio (Blade Height/Chord)	2.25
Design Inlet Flow Angle	-41º
Design Exit Flow Angle	68.5º
Re_{exit}	4.0×10^5

Table 1 Parameters of the Low Speed Linear Cascade

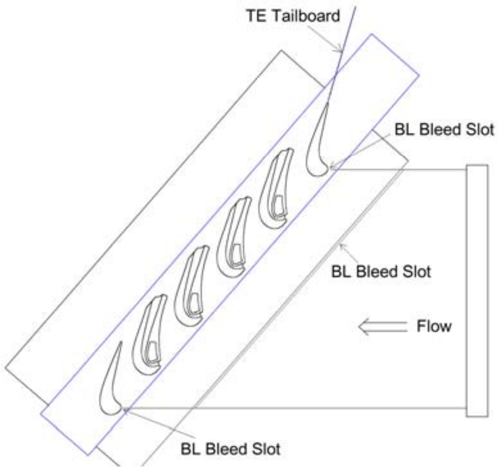

Fig. 1 Layout of Cascade

During all of the experiments, the four central blades have the same size of the tip gap. The third blade from the top is cooled. Static pressure tappings are used in the coolant plenum. The coolant mass flow rate is measured by a variable area flow meter with an accuracy of better than 1%. The other three tips are not cooled in any of the experiments. The two end blades have small fixed tip gaps of less than 0.5mm (0.25%C) to allow the movement of the traversable casing endwall. The endwall is moved in the tangential direction by a stepper motor. The inlet boundary layer of the cascade is measured with a flattened boundary layer pitot probe, which has a width of 1.8 mm and a thickness of 0.6 mm. The inlet boundary layer probe is traversed with the movable endwall to measure the inlet boundary at 35% axial chord upstream of the blade leading edge. A row of 14 static pressure tappings are placed on the movable endwall at different axial locations. By traversing the endwall in the pitchwise direction, the static pressure distributions on the endwall are measured.

On the hub wall of the cascade, five static pressure tappings are located at 50 percent of an axial chord upstream of the blade leading edge and five others are placed at 63 percent of an axial chord downstream of the blade trailing edge. Three pitot tubes, which are located at 50 percent of an axial chord upstream of the cascade, measure the free stream inlet stagnation pressure of the cascade. The temperature of the inlet flow is measured by a thermocouple near the exit of the wind tunnel.

A calibrated 90 degree pyramid five-hole probe is traversed on a plane that is located 45 percent of the axial chord downstream of the blade trailing edge to measure the loss of the third blade from the top. A total of 1334 points are used to cover an area of 228mm in the pitchwise direction (1.27 pitches) and up to 140mm away from the endwall in spanwise direction. The losses are evaluated over one pitch.

The distribution of the cooling effectiveness of the winglet tip is obtained by using the Ammonia - Diazo technique, which uses the analogy between the heat and mass transfer. The ammonia gas is mixed with the coolant. It reacted with the chemicals on the diazo paper, which is attached to the blade tip. Depending on the concentration of ammonia, the chemical reaction leaves traces of different darkness on the diazo paper, from which the cooling effectiveness is derived. The Ammonia - Diazo technique used in the current study is the same as that used by Friedrichs et al. [26].

Fig. 2 shows the geometry of the winglet tip with tip film cooling. Winglets exist on both the pressure side and the suction side of the tip. The pressure side winglet leans towards the flow passage. A cavity is located on the pressure side winglet. A gutter is located almost along the camber line of the blade. The depth of the gutter and the cavity is 4%C. The suction side winglet is plain. The cooling holes are located on the near tip region of the blade surface and on the gutter and the cavity of the winglet tip. No cooling hole is located on the top surface of the winglet tip. All the studies described in this paper were carried out at a tip gap of 1.9%C.

Fig. 2 Geometry of Winglet Tip with Tip Film Cooling

NUMERICAL METHODS

The commercial code Fluent 6.3 was used to solve the RANS equations. The Spalart-Allmaras turbulence model was used. ICEMCFD was used to build the meshes. Fig. 4 shows the structured mesh of the winglet tip. This mesh has 9.8 million elements. The maximum growth factor of the mesh is less than 1.3. O-meshes were used around the blade, the tip cavity and the gutter. Inside the tip gap, there are 31 layers of mesh in spanwise direction. There are 71 points across the suction side winglet and more than 100 points across the pressure side winglet. The average Y^+ on the tip is about 1 and the maximum Y^+ on the tip is about 6.

An unstructured mesh was built for the winglet tip with tip film cooling as shown in Fig. 4, because the geometry was too complex to be meshed with a structured mesh in the time that was available. A hexa-core mesh was used in the main flow passage as shown in Fig. 4(a). Prism meshes were used on all of the surfaces to capture the flow pattern near all the walls, even for the inner surfaces of the cooling holes. An average Y^+ of about 1 was achieved in the numerical results. The maximum Y^+ is about 6. In a grid dependency study for a similar problem (Zhou and Hodson [6]), the variation of the tip leakage loss was less than 0.6% of the loss when the average Y^+ on the blade tip was changed from less than 1 to nearly 10. According to Zhou and Hodson [27], the variation of the heat transfer coefficient is less than 10% when the average tip Y^+ changes from about 0.5 to nearly 6.

Periodic boundary conditions were applied to a single blade to simulate a row of blades. The inlet of the computational domain is located 1.2 axial chords upstream the blade leading edge. No boundary layer was applied at the inlet because the boundary layer bleed slot of the cascade was also located at this position in the experiment. The boundary layer develops as the flow enters the test section.

The free stream stagnation pressure of 660Pa-gauge was applied at the inlet of the cascade. The inlet turbulence intensity in the experiment and the numerical simulation was 0.5%. No boundary layer was applied at the inlet because the boundary layer bleed slot of the cascade is also located at this position in the experiment. The boundary layer develops as the flow enters the test section.

The predicted boundary layer at 35% axial chord upstream of the blade leading edge was compared with the measurement. The CFD predicted a boundary layer with a 99% thickness of 2%C and a shape factor of 1.3. The measurement at this location yielded a 99% thickness of 2.5%C and a shape factor of 1.26. The displacement thickness is predicted to be 0.26%C and is 0.31%C in the experiment.

The outlet of the computational domain is 1.6 axial chords downstream of the trailing edge of the blade. Atmospheric pressure (0 Pa-gauge) was applied at the exit of the computational domain. The Reynolds number was 4.0×10^5 based on the blade chord and the exit conditions. No slip boundary conditions were applied to all walls. Since the tip leakage flow only affects the near tip region of the flow, a span of 140mm (70%C) from the tip was considered. When considering the tip leakage loss, an effective span of 1.34 chords is used. A symmetry boundary condition was used for the 'hub' of the computational domain. The coolant was defined by applying a stagnation pressure at the inlet of the coolant plenum, which provides an engine representative coolant mass flow ratio.

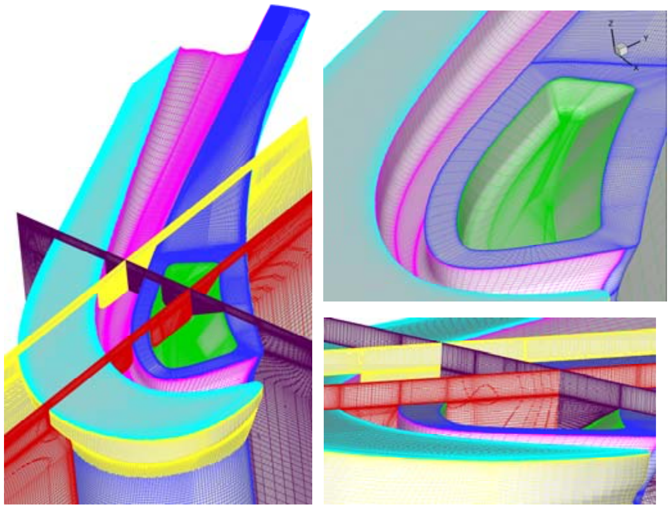

(a) Over View (b) Details of Mesh
Fig. 3 Mesh of Winglet Tip without Tip Film Cooling

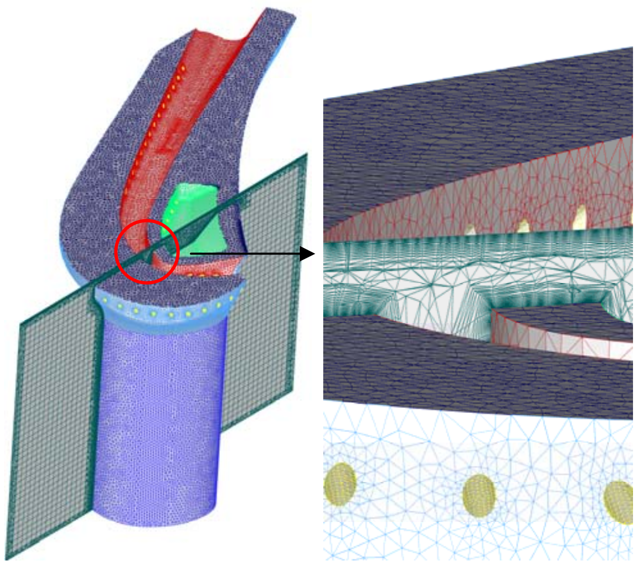

(a) Over View (b) Mesh in Tip Gap
Fig. 4 Mesh of Winglet Tip with Tip Film Cooling

LOSS DEFINITION

After the tip leakage flow exits from the tip gap, the tip leakage flow mixes with the passage flow and creates a loss.

The flow details at a plane downstream of the cascade were obtained from the experiment or CFD data. The mixing downstream of this plane also creates a loss. To take this into account, mixing calculations were carried out. The mixing calculation is conducted using a control volume and assuming that the flow mixes to uniform conditions at constant area without external forces. The way of calculating the mixed out loss can be found in Greitzer et al. [28] The effective span used in the calculation is 1.34 Chord.

The total loss coefficient is defined as

$$Y_{p\_total} = (p_{01\_ref} - p_{03})/(p_{01\_ref} - p_3) \qquad \textbf{Eq. 1}$$

where p_{01_ref} is the reference stagnation pressure, p_{03} is the stagnation pressure at the mixed-out exit plane, and p_3 is the static pressure at the mixed-out exit plane.

For the loss calculation of the tips with tip film cooling, the stagnation pressure of the coolant should be taken into account. So, the reference stagnation pressure p_{01_ref} is defined as

$$p_{01\_ref} = (\dot{m}_m \cdot p_{01} + \dot{m}_c \cdot p_{0c})/(\dot{m}_m + \dot{m}_c) \qquad \textbf{Eq. 2}$$

where $\dot{m}_m$ is the mass flow rate at the inlet of the cascade, and $\dot{m}_c$ is the mass flow rate of the coolant, p_{01} is the free stream stagnation pressure at the cascade inlet, and p_{0c} is the average stagnation pressure at the coolant inlet. For tips without tip film cooling, $\dot{m}_c = 0$.

The coolant mass flow ratio is defined as

$$M_c = \dot{m}_c / \dot{m}_m \qquad \textbf{Eq. 3}$$

where $\dot{m}_c$ is the coolant mass flow rate, $\dot{m}_m$ is the cascade inlet mass flow rate based on an effective span.

The tip leakage loss was obtained by subtracting the profile loss from the total mixed-out loss. The profile loss is obtained as:

$$Y_{p\_profile} = (p_{01} - p_{03\_prof})/(p_{01} - p_3) \qquad \textbf{Eq. 4}$$

where p_{03_prof} is the mixed-out stagnation pressure coefficient at the mid-span. The profile loss coefficient of the experiment is 0.032±0.002 and the predicted value is 0.046. The blade profile loss is over predicted because in the numerical simulation, the flow is fully turbulent, while in real case, boundary layer transition happens on the blade surface. The uncertainty of the tip leakage loss obtained in the experiments was better than 0.002.

RESULTS AND DISCUSSIONS

Blade Surface Static Pressure Coefficient

Fig. 5 shows the predicted static pressure coefficient on the blade surface. The static pressure coefficient is plotted against the axial chord in Fig. 5(a) and against the tangential chord in Fig. 5(b).

Fig. 5(a) shows that the static pressure coefficients on the pressure side surface of the blade from about 10 percent of the axial chord to about 40 percent of the axial chord are almost zero. After 40% of the axial chord, the flow accelerates up to the trailing edge on the blade pressure side. On the suction side of the blade, the flow accelerates to around 30% of the axial chord and then gradually decelerates towards the trailing edge. Fig. 5(b) gives a better presentation of the driving pressure difference of the tip leakage flow, because the direction of the tip leakage flow is closer to the axial direction rather than the tangential direction.

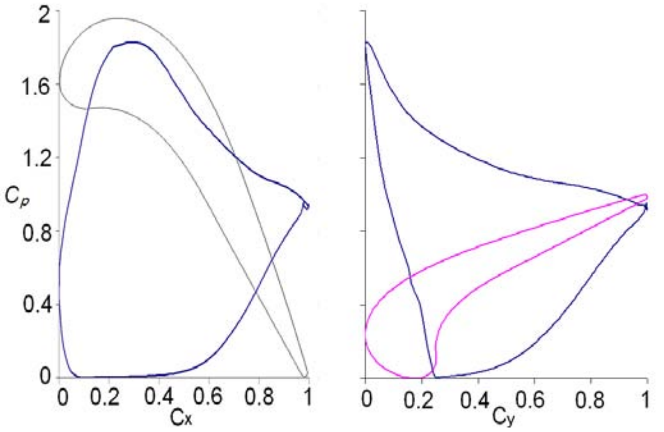

Fig. 5 Mid-span C_p distribution, CFD

CFD validation – Stationary Endwall

Fig. 6 shows the experimental and CFD results of the static pressure distribution on the endwall over the winglet tip. After the flow enters the tip gap, it separates near the pressure side edge of the tip. The region marked 'S', which has a high static pressure coefficient along the blade pressure side is the area over the separation zone, where the flow accelerates. This is well predicted.

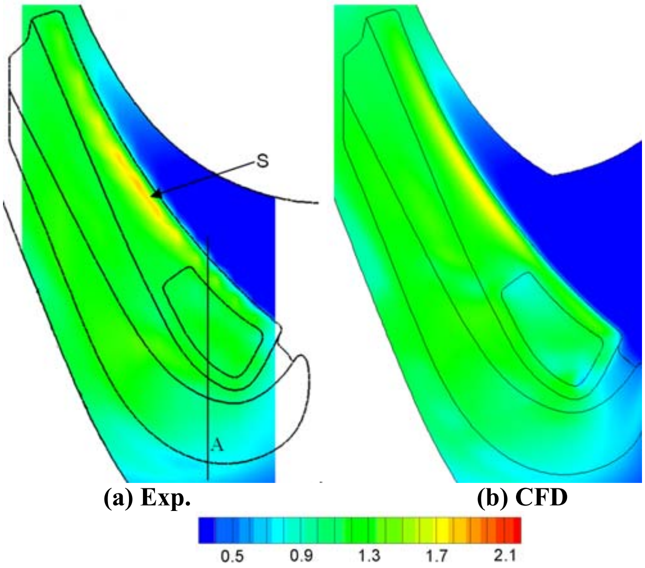

Fig. 6 C_p Distribution on Endwall, Winglet Tip, τ=1.9%C, Stationary Endwall

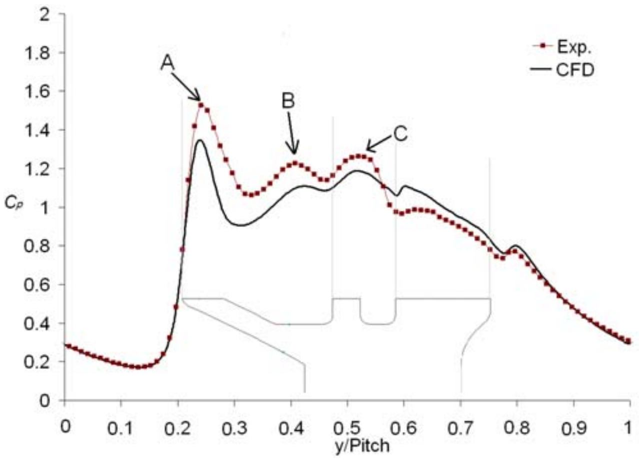

Fig. 7 Endwall C_p Distribution at line 'A' of Fig. 6, Winglet Tip, Stationary Endwall, Exp.

A detailed comparison of the measured and predicted static pressure coefficients on the endwall is shown in Fig. 7, where the values along the line 'A' of Fig. 6 (a) are presented. The CFD predicted the flow separation near the pressure side corner correctly, as show by 'A' in Fig. 7. The peak static pressure coefficient at location 'B' is due to the leakage contraction over the vortex which forms in the pressure side cavity. The leakage flow undergoes another contraction over the middle squealer as shown by 'C' in Fig. 7. The CFD under predicted the static pressure coefficients at position 'A', 'B' and 'C', and over predicted the static pressure coefficient over the suction side winglet.

For the winglet, the pressure drops over each squealer, so it is difficult to quantify the difference in the discharge coefficient between the CFD and the experiment. Based on equivalent data for a flat tip at the same plane shown in Fig. 7, the CFD was found to under predicts the discharge coefficient by 3% using the mixing model in Moore and Tilton [29].

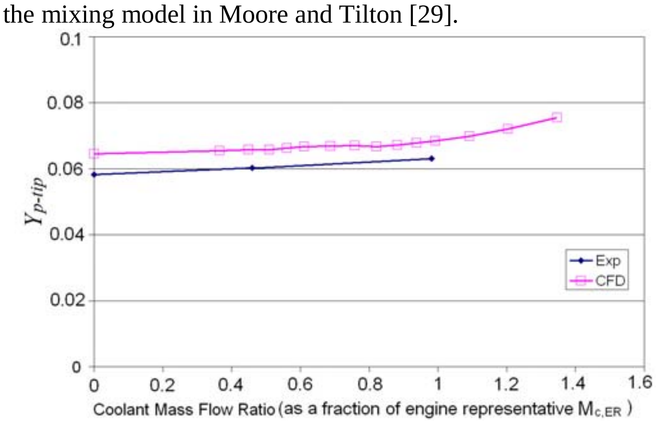

Fig. 8 Tip Leakage Loss of Winglet Tip, Stationary Endwall

Fig. 8 shows both the predicted and the measured tip leakage loss of the winglet tip. Both the experimental and numerical results show that the tip leakage loss of the winglet tip increases with the coolant mass flow ratio. The tip leakage loss increases notably when the coolant mass flow ratio is high, because losses generated as the coolant flow enters the cooling holes from the coolant plenum increases. A more detailed discussion can be found in Zhou et al. [30].

Fig. 9compares the experimental and numerical results of the cooling effectiveness on the cooled winglet tip at the engine representative coolant mass flow ratio. In general, the numerical simulation agrees with the experiment, for which data are only available on the top surface of the tip. For the area shown in the experimental results, the average cooling effectiveness is 0.32, which is 11% higher than the CFD results. Both experimental and numerical results show that the cooling effectiveness in areas 'A' 'B' and 'C' of (b) is low. A more detailed discussion can be found in Zhou et al. [30].

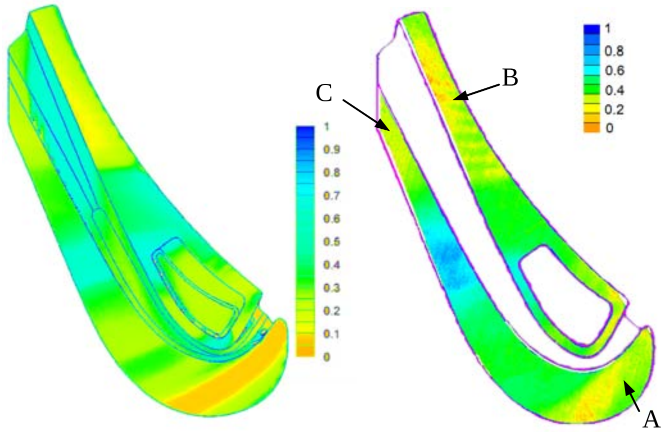

(a) CFD **(b) Exp.**

Fig. 9 Cooling Effectiveness of Winglet Tip with Tip Film Cooling, Stationary Endwall

Endwall Motion

To study the scarping effect due to the endwall motion, the endwall has been moved relative to the blade, while the blade was stationary. The flow coefficient ϕ used in the current research is 0.27. The velocity triangle is shown in Fig. 10. The velocity of the endwall motion U is 40m/s.

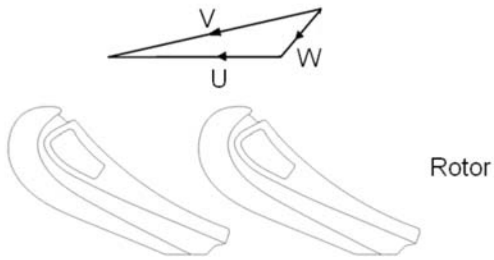

Fig. 10 Velocity Triangle

Flow Field of Tip without Tip Film Cooling

Fig. 11 shows the distribution of the mass flow rate per unit area of the tip leakage flow that exits the tip gap of the winglet tip without tip film cooling. It is plotted against the tangential direction.

Significant differences exist between the cases with the stationary endwall and with the moving endwall. In general, with endwall motion, the tip leakage mass flow rate reduces and the distribution of the leakage mass flow rate per unit area is more uniform. Additionally, the leakage flow exits the tip gap from a location that is further from the leading edge of the blade on the suction side winglet edge with endwall motion. With the stationary endwall, the leakage flow exits the tip gap between point 'S' in Fig. 11 and the trailing edge of the suction side winglet. With a moving endwall, the leakage flow exits the tip gap between point 'M' on the suction side winglet and the trailing edge of the suction side winglet. Between point 'M' and 'S', the passage flow enters the suction side of the tip gap with endwall motion. The leakage mass flow ratio reduces by 42 percent with endwall motion. In this case, the reduction of the tip leakage flow is slightly lower than the experimental results of Yaras and Sjolander [15], in which about a 50 percent reduction in the leakage mass flow rate was obtained by moving the endwall at a flow coefficient of 0.46.

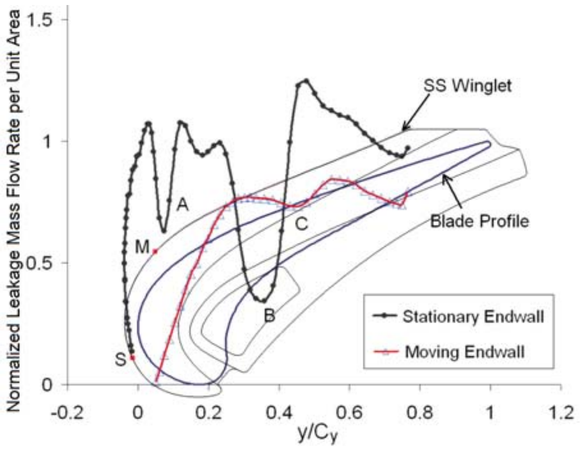

Fig. 11 Leakage Mass Flow Rate per Unit Area that Exits Gap, Winglet Tip without Tip Film Cooling, CFD

Fig. 12 shows the velocity distribution on the plane at the middle of the tip gap with velocity vectors. The velocity is normalized by the velocity at the exit of the cascade. With endwall motion, the distribution of the velocity inside the tip gap changes significantly. For the case with the stationary endwall shown in Fig. 12(a), the flow exits the cavity on the pressure side winglet and separates over the two corners of the cavity. The separation over the corner that creates the low velocity region 'B' can be seen in Fig. 13(a), where the velocity vectors at the cut plane of Fig. 12(a) are plotted.

The endwall motion imposes a tangential component to the velocity of the flow near the endwall. As shown by the velocity vectors in Fig. 12(b), the endwall motion changes the direction of the flow within the tip gap, especially over the suction side winglet. With endwall motion, the blockage near location 'A' in Fig. 12(a) disappears in Fig. 12(b). The blockage created by the flow separation over the other corner of the cavity on the pressure side winglet moves from location 'B' in Fig. 12(a) to location 'C' Fig. 12(b). Additionally, the effect of the reduction in the leakage mass flow rate at location 'C' in Fig. 12(b) is less evident than the effect at location 'B' in Fig. 12(a). This agrees with the results shown in Fig. 11.

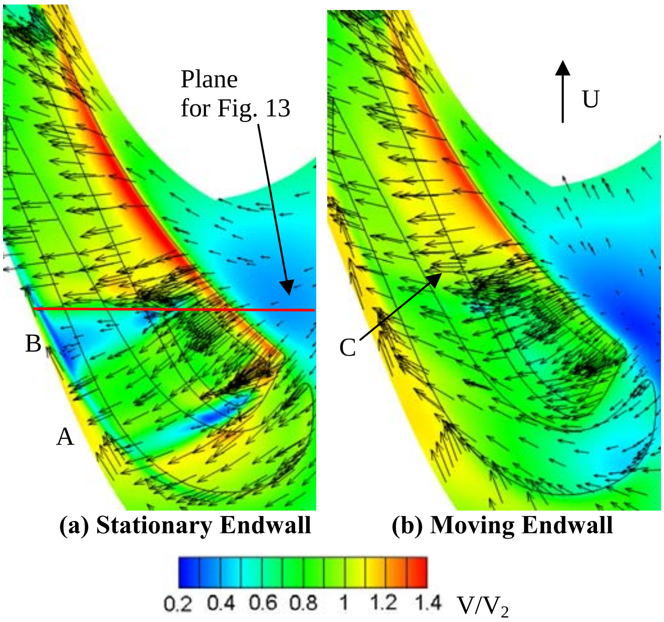

Fig. 12 Velocity Distribution in Middle of Tip Gap, CFD

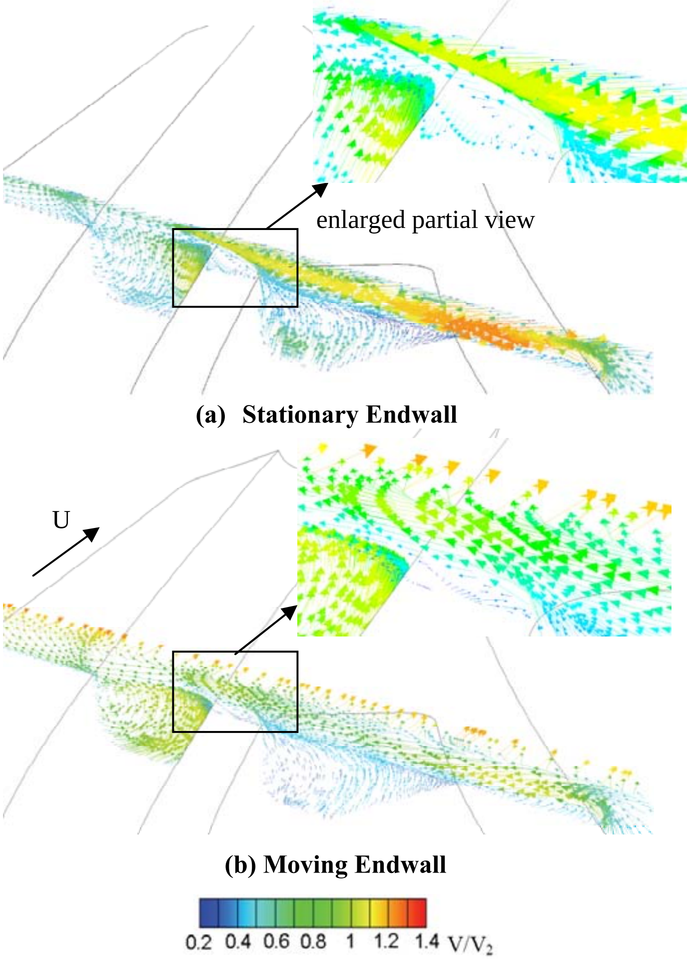

Fig. 13 Velocity Vectors at the Cut Plane of Fig. 12(a), CFD

Fig. 13 shows the velocity vector at the cut plane of Fig. 12(a). As no slip boundary conditions are used on all of the walls, the flow next to the endwall is significantly affected by endwall motion. The endwall motion creates large velocity gradients near the endwall in spanwise direction and results in a viscous force in the tangential direction. The viscous shear affects the tangential components of the velocity vectors near the endwall and changes the distribution of velocity within the tip gap. In Fig. 13(b), the velocity vectors near the endwall have large components in the direction of the moving endwall, which is different from the case with the stationary endwall (Fig. 13a). The velocity magnitude at the vena-contracta near the pressure side inlet of the tip gap is lower with endwall motion than the case where the endwall is stationary. With endwall motion, the sizes of the flow separation zone over the squealer between the cavity and the gutter reduce, which can be seen in the enlarged partial view. The size of the separation zone near the pressure side edge also reduces. This agrees with the experimental results of Yaras and Sjolander [15] and Palafox et al. [19], who showed that the endwall motion reduces the size of the separation zone over the tip.

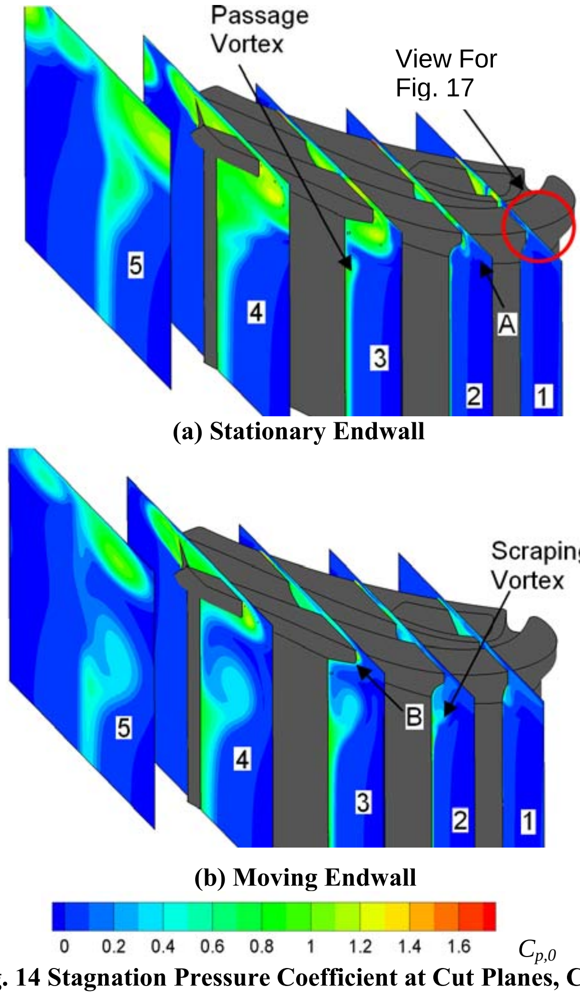

Fig. 14 Stagnation Pressure Coefficient at Cut Planes, CFD

Fig. 14 shows the distribution of the stagnation pressure coefficient ($C_{p,0}$) at several cut planes. Fig. 14 (a) shows the case with the stationary endwall. The leakage flow exits the tip gap and forms a tip leakage vortex. The leakage vortex is clearly seen in the area near 'A' in plane '2' of Fig. 14(a). With the moving endwall, the leakage flow exits from a position further from the leading edge and the tip leakage mass flow ratio reduces. In Fig. 14(b), the vortex due to the leakage flow appears downstream at plane '3' as indicated by 'B' and its size is much smaller than that in the case with the stationary endwall. In plane '2' of Fig. 14(b), a scraping vortex appears near the blade tip due to the scraping effects of the endwall motion. The stagnation pressure coefficient of the scraping vortex is high. The shape of the scraping vortex is significantly different from that of the passage vortex as shown in Fig. 14(a). The scraping vortex also affects the thermal performance of the winglet tip, especially when coolant is used. This will be discussed later. At plane '5', which is just downstream of the blade, the reduced tip leakage vortex and the scraping vortex due to the endwall motion changes the flow field near the endwall significantly. The scraping vortex was also observed by Palafox et al. [25] and Yaras [17].

Fig. 15 shows the distribution of the pitchwise mass averaged stagnation pressure coefficient relative to the blade profile loss at 15% axial chord downstream of the trailing edge. Due to the tip leakage flow, the stagnation pressure coefficient is high near the endwall with the stationary endwall and with the moving endwall. For the winglet tip with the stationary endwall, the passage vortex increases the stagnation pressure coefficient at about 25%C from the endwall in spanwise direction. The stagnation pressure coefficient reaches the level of the stagnation pressure coefficient due to the profile loss at about 45%C from the endwall in spanwise direction for the case with the stationary endwall. The passage vortex no longer exists as a separate vortex with endwall motion.

Fig. 15 shows that the stagnation pressure coefficients near the endwall are smaller when the endwall moves. One reason is that the endwall motion reduces the tip leakage mass flow ratio. Another reason is due to the work input due to the viscous force associated with the moving endwall. At about 45%C from the endwall in the spanwise direction, the stagnation pressure coefficient increases because of the scraping vortex caused by endwall motion. At about 20%C from the endwall in spanwise direction, the stagnation pressure coefficient is lower than the level of the stagnation pressure coefficient due to the blade profile loss. This is mainly because work is done by the shear force imposed by the endwall motion. The work done by the endwall will be accounted for when evaluating the overall net loss.

Fig. 16 shows the spanwise variation of the deviation of the momentum based yaw angle at 15% axial chord downstream of the cascade. With endwall motion, the deviation of the flow angle near the endwall reduces significantly mainly because of the reduction of the tip leakage flow. However, at about 40%C from the endwall in spanwise direction, the scraping vortex reduces the turning of the flow. The increase of the flow turning angle at 20%C from the endwall in the spanwise direction is due to the work input by the endwall motion. Because the size of the tip leakage vortex is reduced and the scraping vortex is formed, the flow pattern downstream of the cascade changes with endwall motion. The changes may affect the behavior of the downstream component in the turbine.

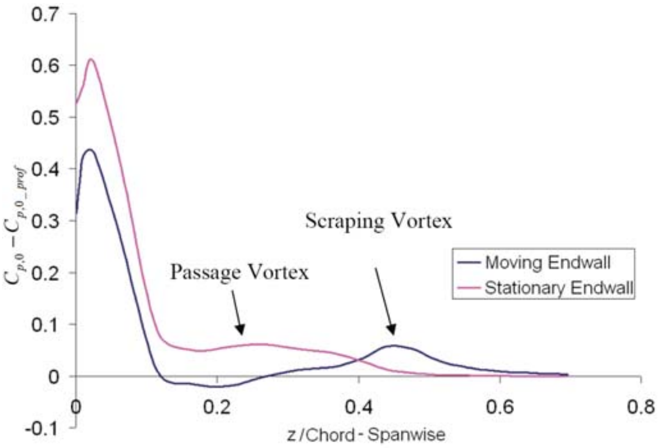

Fig. 15 $C_{p,0} - C_{p,0\_prof}$ **in Spanwise Direction, 15%C_x Downstream, CFD**

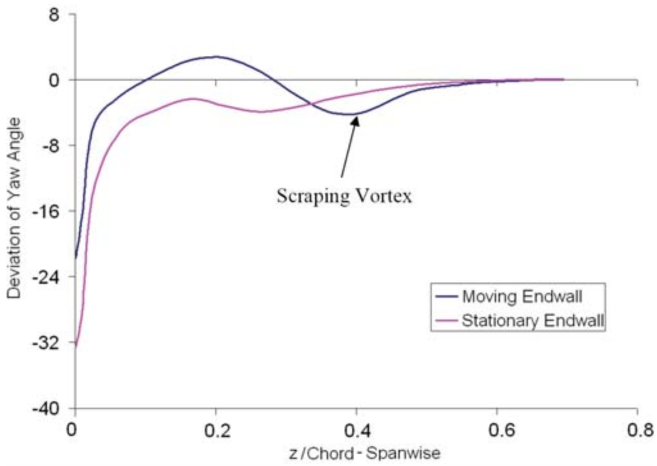

Fig. 16 Deviation of Yaw Angle Relative to Midspan in Spanwise Direction, 15%C_x Downstream, CFD

Fig. 17 shows 3D velocity vectors at plane '1' in Fig. 14(a) near the tip gap exit of the suction side winglet. Two dimensional streamlines on this plane are also presented. Fig. 17(a) shows the case with the stationary endwall. The flow exits the tip gap at this cut plane and forms the tip leakage vortex. Near the endwall, most of the velocity vectors have large components in the axial direction. Fig. 17(b) shows the case with the moving endwall. The velocity vectors near the endwall shows large tangential components in the direction of the endwall motion. The 2D flow path lines show that rather than exiting the tip gap, the flow enters the tip gap at this plane due to the scraping effect. The viscous shear force imposed by the endwall motion moves the flow into the tip gap.

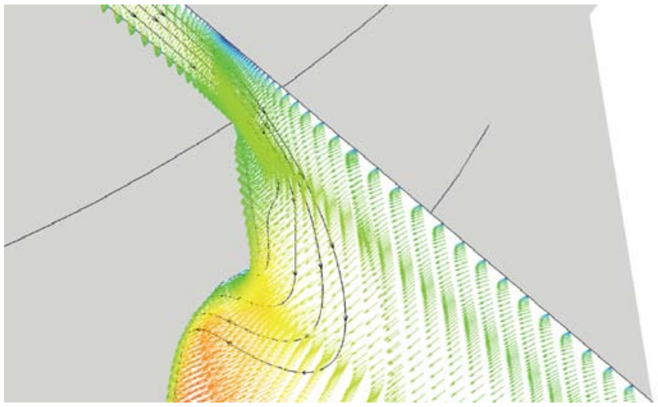

(a) Stationary Endwall

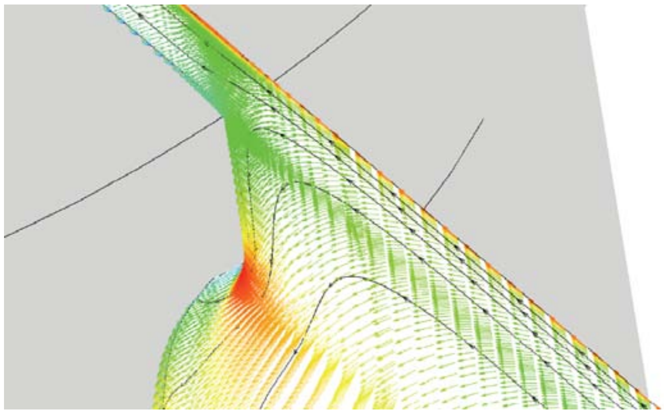

(b) Moving Endwall

Fig. 17 Velocity Vector and 2D Flow Path Lines near Suction Side Winglet, View of Plane '1' in Fig. 14, 24%C_x, CFD

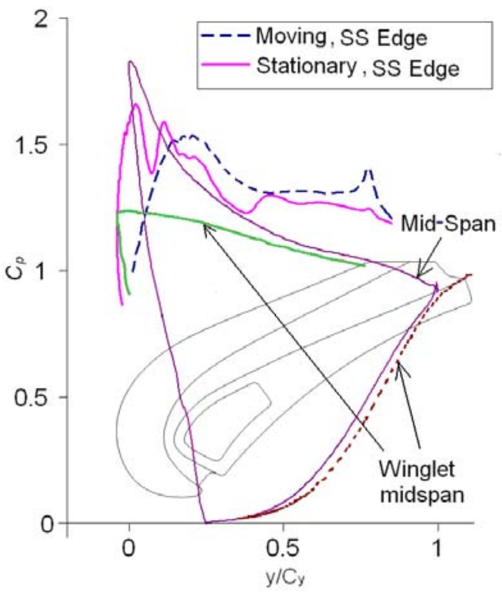

Fig. 18 Static Pressure Distribution of Winglet Tip, CFD

Fig. 18 presents the distribution of the static pressure coefficients of the winglet tip. According to Rains [1], the tip leakage flow mass flow rate is mainly determined by the pressure difference across the tip. The driving pressure difference is mainly determined by the static pressures along a projection of the pressure side winglet edge to the midspan and the static pressure at the exit of the suction side winglet. As shown in Fig. 18, the static pressure coefficients on the 'winglet midspan' curve are quite similar to those on the blade pressure side surface at midspan. So, the pressure side winglet does not reduce the driving pressure difference, which agrees with Schabowski and Hodson[2].

Fig. 18 shows that the static pressure coefficients on the 'winglet midspan' curve are lower than those on the blade suction side surface at midspan. This means that the suction side winglet should reduce the driving pressure difference of the tip leakage flow. However, the static pressure field at the exit of the tip gap is affected by the leakage vortex, which has a relatively low static pressure. With a stationary endwall, the static pressure coefficient on the suction side edge of the winglet is higher than those on the 'Winglet midspan' due to the low static pressure in the tip leakage vortex. With endwall motion, the tip leakage vortex is closer to the suction side exit of the tip gap. So, the static pressure at the exit of the tip gap decreases between 15% of the tangential chord to the trailing edge with endwall motion. This slightly increases the driving pressure difference of the tip leakage flow across that part of the blade tip. However, even with the increased driving pressure difference, the tip leakage mass flow ratio of the winglet tip with a moving endwall is still much lower between about 50% of the tangential chord to the trailing edge with endwall motion, as shown in Fig. 11.

Near the leading edge of the suction side winglet, the tip leakage flow exits the tip gap only when the endwall is stationary, so the static pressure near the leading edge of the suction side winglet is lower with a stationary endwall than that with a moving endwall. The endwall motion reduces the tip leakage flow mainly by the action of its shear force. Compared with the effects of viscous force due to the endwall motion, the effects due to the change in the driving pressure difference of the tip leakage flow are small.

Tip Leakage Loss

The total mixed-out loss was calculated by assuming that the cascade exit flow was fully mixed out at constant area. The effective span used in the calculation is 1.34 chords. As the endwall moves relatively to the blade tip, work is done by the endwall to the flow. To calculate the loss, the work done by the endwall has to be considered as shown below. The overall stagnation pressure loss is given by:

$$p_{01} - p_{03} = Y_{p\_total} \cdot (p_{01} - p_3) + \rho \cdot \dot{W} / \dot{m}_{passage} \qquad \textbf{Eq. 5}$$

where Y_{p_total} represents the total loss coefficient, $\dot{W}$ is the viscous work done by the moving endwall and $\dot{m}_{passage}$ is the mass flow rate. The work of the endwall was evaluated for the computational domain using

$$\dot{W} = \vec{F}_{endwall} \cdot \vec{V}_{endwall} \qquad \textbf{Eq. 6}$$

where $\vec{F}_{endwall}$ is the viscous shear force imposed by the endwall on the fluid and $\vec{V}_{endwall}$ is the velocity of the endwall. The tip leakage loss coefficient is calculated by subtracting the profile loss coefficient from the total loss Y_{p_total}. In Eq. 5, the term of $\rho \cdot \dot{W} / \dot{m}_{passage}$ due to the viscous work of the endwall motion is about 15% of the change in the stagnation pressure $(p_{01} - p_{03})$.

With endwall motion, the tip leakage loss coefficient is 0.052, which is 15% lower than the tip leakage loss coefficient with a stationary endwall. The proportional reduction of the tip leakage loss is less than the reduction of the tip leakage mass flow ratio (42%), partly because of the scraping vortex due to the endwall motion, which creates a loss, and because the work input is viscous. Tallman et al. [18] found that although the tip leakage flow reduces with endwall motion, the change of the overall losses was small.

Thermal Performance

Winglet Tip without Film Cooling

Fig. 19 shows the distribution of the Nusselt number on the winglet tip. Fig. 19(a) shows the case of the winglet tip with the stationary endwall. The Nusselt number on the areas marked 'C' and 'D' are low. This is mainly because the velocity of the flow over these areas is low, as shown in Fig. 12(a). The Nusselt numbers between areas 'C' and 'D' are also quite low, because the velocities of the leakage flow over these areas are reduced by the cavity on the pressure side winglet of the tip. The Nusselt number near 'G' is high, because the velocity of the flow is high over this area. Similarly, high Nusselt numbers appear near 'H'. The Nusselt numbers near the leading edge of the blade tip are high, as marked by 'E'.

Fig. 19(b) shows the case with the moving endwall, which differs significantly from the case shown in Fig. 19(a). The most striking difference appears in area 'A' of Fig. 19(b) near the leading edge of the suction side winglet. The Nusselt numbers in this region are much lower than those in the case shown in Fig. 19(a). The main reason is that the flow velocity over this area is low with the moving endwall, as shown in Fig. 12(b). Because less flow enters the tip gap with the moving endwall, the velocity within the tip gap reduces. As a result, the Nusselt number on the winglet tip reduces by 14% with endwall motion. The reduction of the Nusselt numbers in the gutter is relatively small, because the flow in the gutter is less affected by the endwall motion than other parts of the winglet tip. At an engine representative condition, O'Dowd et al. [11] also observed that the relative endwall motion resulted in significant change near the leading of the blade tip, where the flow is subsonic.

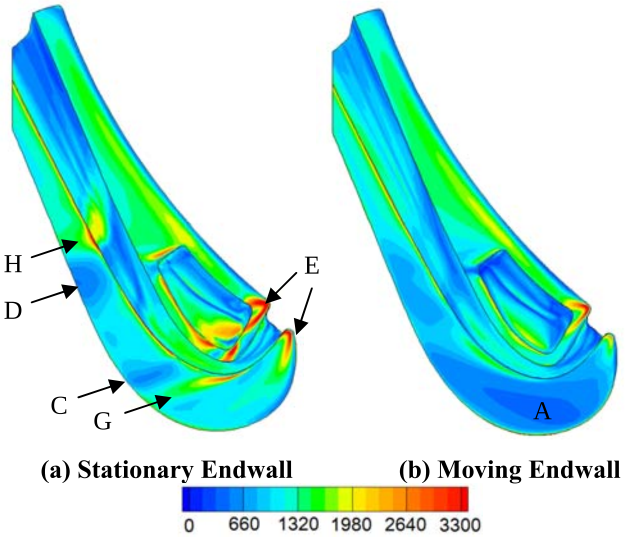

(a) Stationary Endwall **(b) Moving Endwall**

Fig. 19 Nusselt number on Winglet Tip, CFD

Fig. 20 shows the distribution of the Nusselt numbers on the pressure side surface and the suction side surface of the blade. As shown in Fig. 20(a) and (b), near the blade leading edge, the Nusselt numbers near the pressure side edge of the tip reduce with endwall motion. This is because the tip leakage mass flow rate reduces significantly near the leading edge as shown in Fig. 11. Apart from that, the effects of the endwall motion on the distribution of the Nusselt number on the blade pressure side are not very large.

The impingement of the tip leakage vortex results in high Nusselt numbers on the blade suction side surface. As shown by Fig. 14(a) and (b), with endwall motion, the size of the tip leakage vortex reduces and the position of the tip leakage vortex appears closer to the tip of the blade. So, Fig. 20(c) and (d) show that the leakage vortex impinges in a position that is closer to the tip of the blade in spanwise direction with the moving endwall. The area 'B' with higher Nusselt numbers in Fig. 20(d) is a result of the impingement of the tip leakage flow. The Nusselt number in area 'H' of Fig. 20(c) reduces due to the endwall motion, because the effect of the tip leakage flow impingement reduces. As shown in Fig. 20(c) and (d), the scraping vortex changes the Nusselt number distribution on the suction side surface of the blade.

The above results were obtained with a structured mesh. An unstructured mesh was also built for the winglet tip without tip film cooling. The average Nusselt number of the winglet tip without tip film cooling that was predicted with the unstructured mesh is less than 5% lower than that of the structured mesh in cases with a stationary endwall or a moving endwall. Both meshes provide consistent predictions of the aero-thermal performance of the winglet tip without tip film cooling.

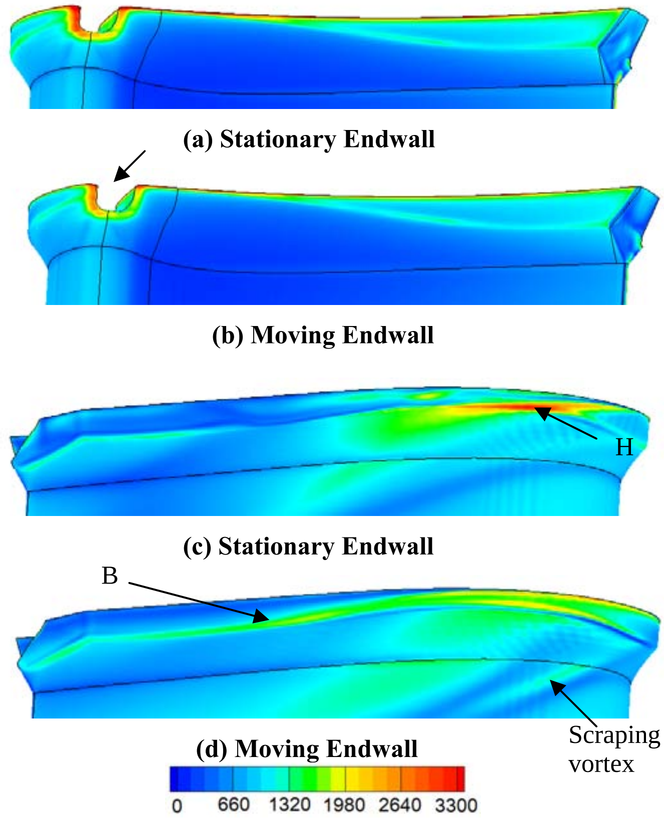

Fig. 20 Distribution of Nusselt number on Surfaces of Winglet Tip, CFD

Winglet Tip with Tip Film Cooling

In high pressure turbines, the blade tips usually have to be cooled. To study the effects of endwall motion on the thermal performance of the winglet tip with tip film cooling, the inlet of the coolant was defined by the same stagnation pressure for both the cases with the stationary endwall and moving endwall. The endwall motion slightly reduces the coolant mass flow ratio by about 2% due to the change of the static pressure at the exit of the cooling holes, especially for the holes on the suction side winglet.

Fig. 21 shows the distribution of the cooling effectiveness on the winglet tip. Fig. 21(a) shows the same data as Fig. 9(a). The distributions of the cooling effectiveness, which are related to the flow paths of the coolant, reflect the changes of the flow direction within the tip gap due to endwall motion (refer to velocity vectors in Fig. 12). Compared to the case with the stationary endwall, the distribution of the cooling effectiveness on the winglet tip significantly changes with the endwall motion, especially near the leading edge of the suction side winglet as marked by 'A' in Fig. 21(b). With endwall motion, the tip leakage mass flow ratio reduces by about 40%, but the coolant mass flow ratio is almost unchanged. Therefore, the ratio of the coolant mass flow rate to the leakage mass flow rate increases significantly. However, less coolant from the pressure side surface of the blade enters the tip gap as the tip leakage mass flow reduces. Nevertheless, the ratio of the coolant ejected from the cavity and the gutter to the leakage flow increases. This increases the cooling effectiveness in areas such as the cavity and the gutter of the winglet tip. As a result, the average cooling effectiveness on the winglet tip increases by about 9% with endwall motion.

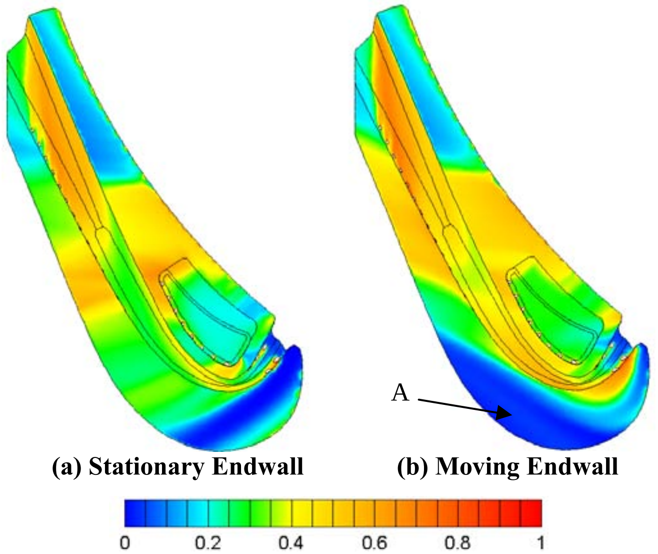

Fig. 21 Cooling Effectiveness on Winglet Tip with Tip Film Cooling, CFD

Fig. 22 shows the distribution of the cooling effectiveness on the pressure side surface and the suction side surface of the blade. The endwall motion has a small effect on the distribution of the cooling effectiveness of the blade pressure side surface, as shown in Fig. 22(a) and (b). In contrast, the distribution of the cooling effectiveness on the blade suction side surface changes significantly with endwall motion. With the stationary endwall, as shown in Fig. 22(c), the area 'A' is effectively cooled by the coolant both from the holes on the suction side surface and across the tip gap. However, in the case with the moving endwall shown in Fig. 22(d), this area is not cooled by either the coolant across the tip or the coolant from the holes on the suction side surface. Because of the endwall motion, the coolant over the tip exits at location 'B' in Fig. 22(d). Due to the reduced size of the tip leakage vortex, the coolant that exits the tip gap cools a smaller area on the suction side surface with the moving endwall.

Near the leading edge of the suction side surface, the distributions of the coolant are significantly different between the cases with the stationary endwall and the moving endwall. In Fig. 22(d), after the coolant exits the cooling holes on the suction side surface, it covers area 'C', which is very different from that in the case with the stationary endwall. This is due to the scraping effect created by the endwall motion and will be explained with the aid of Fig. 23.

Fig. 23(a) and (b) show the distribution of the cooling effectiveness on the blade suction side surface. These show the leading edge of the winglet tip viewed in the direction shown in Fig. 22(d). In Fig. 23(a), with the stationary endwall, some of the coolant from the holes near the leading edge enters the tip gap. The coolant from the holes located further from the leading edge does not enter the tip gap, but cools the near tip region of the suction side surface. With endwall motion, Fig. 23(b) shows that the coolant exits from the coolant holes and mixes with the flow that forms the scraping vortex. This results in a significant change in the distribution of the cooling effectiveness near the leading edge of the blade suction side surface.

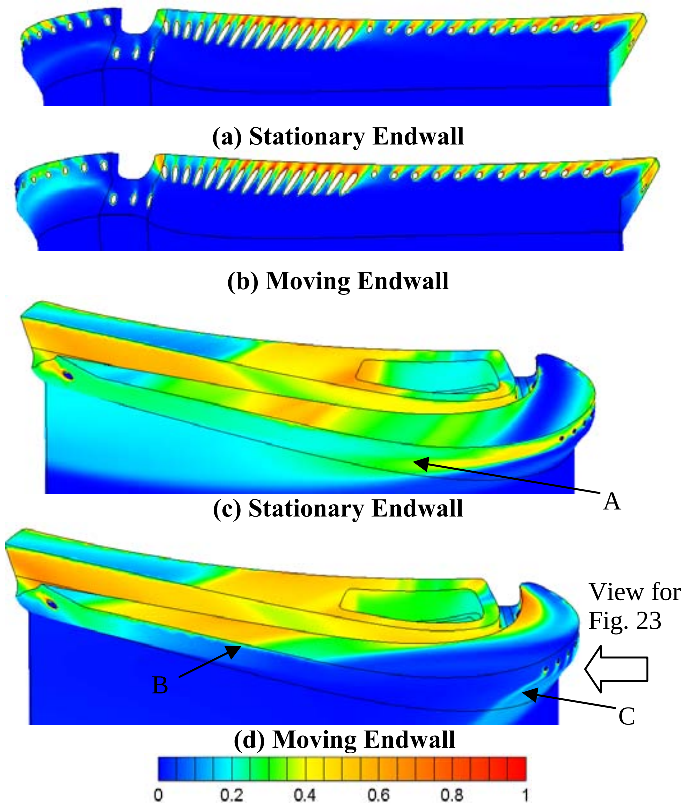

Fig. 22 Cooling Effectiveness on Blade Surfaces, CFD

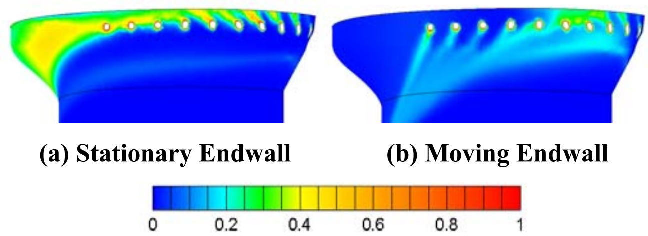

Fig. 23 Cooling Effectiveness, CFD, View from Leading Edge (see Fig. 22d)

The heat flux rate per unit area indicates the absolute rate at which heat enters the blade per unit area per temperature difference. If the value is negative, it indicates that the heat transfers from the blade to the external flow. For cooled tips, the temperatures of the inlet flow, the coolant and the walls were based on the non-dimensional engine temperature Θ_E of 1.5, which is the same as that used in Newton [13].

Fig. 24(a) and (b) shows the distribution of the heat flux near the pressure side of the blade tip. With a stationary endwall (Fig. 24a), the heat flux rate between the cooling holes in area ‘A’ is much higher than that on the other areas of of the blade tip due to low cooling effectiveness and high Nusselt number. In Fig. 24 (b), the peak heat flux rate near the leading edge marked ‘A’ is reduced when compared with the winglet tip with the stationary endwall shown in Fig. 24(a). This is because of the reduction of the local Nusselt numbers due to the endwall motion, which significantly reduces the leakage mass flow rate near the leading edge. Nevertheless, the heat flux rate near the leading edge is still quite high.

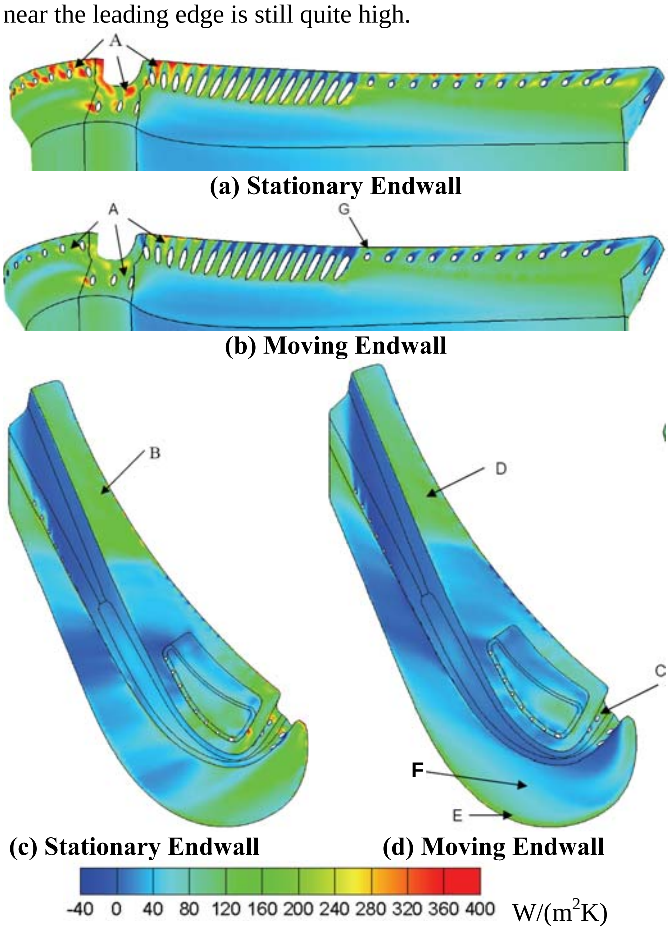

Fig. 24 Heat Flux Rate h_{rate} of Winglet Tip with Tip Film Cooling, CFD

Fig. 24(c) and (d) shows the distribution of the heat flux on the tip. Although area ‘B’ in Fig. 24(c) also has low cooling effectiveness, the heat flux rate on this area is less than half of that in area ‘A’ in Fig. 24(a) due to the lower Nusselt numbers.

Although area ‘F’ in Fig. 24(d) suffers from low cooling effectiveness, this area also has low Nusselt numbers, as shown in Fig. 19(b). As a result, the heat flux rate of this area (‘F’ in Fig. 24d) is not very high except for the area near the edge of the suction side winglet (‘E’ in Fig. 24d). Here, the Nusselt number is not low and the cooling effectiveness is very low. Around area ‘C’ in Fig. 24(d), high heat flux rates also appear on the squealer of the cavity and near the leading edge of the gutter. The area around ‘D’ on the pressure side winglet has high heat flux rate due to the lack of coolant from the holes on the pressure side surface corresponding to this area. With the increased cooling effectiveness and the reduced Nusselt numbers, the overall heat flux rate on the winglet tip with tip film cooling reduces by 31% with endwall motion.

CONCLUSIONS

The effects of endwall motion on the aero-thermal performance of both winglet tips with and without tip film cooling were studied at a tip gap of 1.9%C.

Experimental and numerical methods were used to study the cases with a stationary endwall. The static pressure distribution on the endwall, the tip leakage loss with different coolant mass flow ratios and the cooling effectiveness on the blade tip were presented. The predicted results compare favorably with the experimental results. The CFD tool then was used to study the effects of endwall motion.

The endwall motion imposes a tangential force on the velocity of the flow near the endwall. With endwall motion, the distribution of the tip leakage mass flow rate per unit area that exits the tip gap, as well as the flow pattern within the tip gap, changes significantly. The tip leakage mass flow ratio that exits the tip gap from the suction side edge reduces by about 42% with endwall motion. Due to the moving endwall, a scraping vortex is formed and creates a loss. Overall, the tip leakage loss of the winglet tip reduces by about 15% with endwall motion. With endwall motion, the flow field downstream of the cascade changes, because the size of the tip leakage vortex reduces and the scraping vortex appears.

With endwall motion, the reduced tip leakage mass flow ratio and the changed flow pattern within the tip gap significantly changes the distribution of Nusselt numbers on the winglet tip. For the winglet tip without tip film cooling, the Nusselt number decreases by 14% with endwall motion. This is mainly due to the reduction in the tip leakage mass flow ratio, which reduces the leakage velocity over the tip.

On the winglet tip with tip film cooling, the cooling effectiveness increases by 9% with endwall motion. Combined with the reduced Nusselt number, the heat flux on the winglet tip reduces by 31% with endwall motion. The cooling effectiveness on the near tip region of the pressure side remains almost unchanged, but the heat flux rate in this area reduces. This is because of the reduced tip leakage mass flow. With the moving endwall, the distribution of the cooling effectiveness on the suction side surface of the blade is significantly affected by the scraping vortex. Certain areas on the suction side surface that are well protected by the coolant flow with a stationary endwall are left unprotected with endwall motion. Therefore, the effects of the endwall motion should be considered during the design of the blade tip.

ACKNOWLEDGMENTS

This work is sponsored by Rolls-Royce and the Department of Trade and Industry. The authors wish to thank Rolls-Royce for the permission to publish this work.

REFERENCES

[1] Rains D. A., “Tip clearance flows in axial flow compressors and pumps”, PhD thesis, California Institute of Technology, 1954

[2] Schabowski, Zbigniew, and Hodson, Howard, “The Reduction of Over Tip Leakage Loss in Unshrouded Axial Turbines Using Winglet and Squealers”, ASME Paper, GT2007-27623, 2007.

[3] Liu, H. C., Booth, T. C., and Tall, W. A., “An Application of 3-D Viscous Flow Analysis to the Design of a Low-Aspect-Ratio Turbine,” ASME Paper 79-GT-53, 1979.

[4] Harvey, N., Newman, D. and Haselbach, F., “An Investigation Into a Novel Turbine Rotor Winglet. Part 1: Design and Model Rig Test Results”, GT2006-90456, 2006

[5] Harvey, N. W., “Turbine Blade Tip Design and Tip Clearance Treatment”, VKI Lecture Series 2004

[6] Zhou, C., and Hodson, H., “The Tip Leakage Flow of an Unshrouded High Pressure Turbine Blade With Tip Cooling”, ASME paper GT 2009-59637, 2009

[7] Hofer, T., Arts, T., “Aerodynamic Investigation of the Tip Leakage Flow for Blades with Different Tip Squealer Geometries at Transonic Conditions”, ASME paper GT2009-59909, 2009

[8] Rao N., and Camci, C., “Axial Flow Turbine Tip Desensitization by Injection from a Tip Trench. Part 1- Effect of Injection Mass Flow Rate,” ASME Paper GT2004-53256 2004a.

[9] Bunker, “Axial Turbine Blade Tips: Function, Design, and Durability”, Journal of Propulsion and Power, Vol. 22, No. 2, 271-285, 2006

[10] Papa, M., Glodstein., R. J., Gori, F., “Effects of Tip Geometry and Tip Clearance on the Mass/Heat Transfer From a Large-Scale Gas Turbine Blade”, Journal of Turbomachinery, Vol.125, pp90-96, 2003.

[11] O’Dowd, D. O., Zhang, Q., He, L., Oldfield, M., Ligrani, P., Cheong, B., Tibbott, I., “Aero-Thermal Performance of a Winglet at Engine Representative Mach and Reynolds Numbers”, GT2010-22794, 2010

[12] Christophel, J. R., Thole, K. A., and Cunha, F. J., “Cooling the Tip of a Turbine Blade Using Pressure Side Holes – Part 1: Adiabatic Effectiveness Measurements”, Journal of Turbomachinery, Vol. 127, pp270-277, 2005

[13] Newton, P. J., Lock, G. D., Krishnababu, S.K., Hodson, H.P., Dawes, W.N., Hannis, J., and Whitney, C., 2007, “Aero-thermal investigation of tip leakage flow in axial flow turbines Part III- film cooling” ASME Paper No. GT-2007-27368, 2007.

[14] Ahn, J., Mhertras, S., Han, J. C., “ Film-Cooling Effectiveness on a Gas Turbine Blade Tip Using Pressure-Sensitive Paint ”, Journal of Turbomachinery, Vol. 127, pp.521-530, 2005.

[15] Yaras M. I., Sjolander S. A. “Effects of Simulated Rotation on Tip Leakage in a Planar Cascade of Turbine Blades: Part I – Tip Gap Flow”, ASME Journal of Turbomachinery, Vol. 114, pp. 652-659, July 1992

[16] Graham, J. A. H. “Investigation of a Tip Clearance Cascade in a Water Analogy Rig”, Journal of Turbomachinery, Vol. 108, pp 38-46, 1986.

[17] Yaras M. I., Sjolander S. A., Kind R. J., “Effects of Simulated Rotation on Tip Leakage in a Planar Cascade of Turbine Blades: Part II – Downstream Flow Field and Blade Loading”, ASME Journal of Turbomachinery, Vol. 114, pp. 660-667, July 1992

[18] Tallman J., and Lakshminarayana B., “Numerical Simulation of Tip Leakage Flows in Axial Flow Turbines, With Emphasis on Flow Physics: Part II—Effect of Outer Casing Relative Motion”, Journal of Turbomachinery, Vol. 123, pp323-333, 2001.

[19] Palafox P., Oldfield M. L. G., LaGraff J. E., Jones T. V., “PIV Maps of Tip Leakage and Secondary Flow Fields on a Low Speed Turbine Blade Cascade with Moving Endwall”, ASME Paper GT2005-68189, 2005.

[20] Krishnababu, S. K., Dawes, W. N., Hodson, H. P., Lock, G. D., Hannis, J., and Whitney, C., “Aero-thermal investigation of tip leakage flow in axial flow turbines Part II-Effect of relative casing motion” ASME Paper No. GT-2007-27957, 2007

[21] McCarter, A. A., Xiao, X., Lakshminarayana, B., “Tip Clearance Effects in a Turbine Rotor: Part 2 – Velocity Field and Flow Physics”, Journal of Turbomachinery, Vol. 123, pp305-313, 2001

[22] Yang, D., Yu, X., Feng, Z., “Investigation of Leakage Flow and Heat Transfer in a Gas Turbine Blade Tip With Emphasis on the Effect of Rotation”, Journal of Turbomachinery, Vol. 132, 041010(9 pages), 2010

[23] Srinivasan, V., and Goldstein, R. J., “Effect of Endwall Motion on Blade Tip Heat Transfer”, Journal of Turbomachinery, Vol. 125, pp267-273, 2003

[24] Rhee, D.H., Cho, H. H., “Local Heat/Mass Transfer Characteristics on a Rotating Blade with Flat tip in a Low-Speed Annular Cascade – Part 2: Tip and Shroud”, Journal of Turbomachinery, Vol.128, pp110-119, 2006

[25] Palafox P., Oldfield M. L. G., Ireland P. T., Jones T. V., LaGraff J. E., “Blade Tip Heat Transfer and Aerodynamics in a Large Scale Turbine Cascade with Moving Endwall”, ASME Paper GT2006-90425, 2006

[26] Friedrichs, S., Hodson, H., Dawes, W.N., “Distribution of Film-cooling Effectiveness on a Turbine Endwall Measured Using the Ammonia and Diazo Technique”, Journal of Turbomachinery, Vol.118, pp613-621, 1996

[27] Zhou, C., and Hodson, H., “Numerical Investigation of Thermal Performance of Unshrouded HP Turbine Blade Tips”, International Journal of Turbo and Jet Engines, Vol. 26, 2009

[28] Greitzer, E. M., Tan, C. S, Graf, M. B., “Internal Flow”, Cambridge University Press, 2004

[29] Moore, J., and Tilton, J. S., “Tip Leakage Flow in a Linear Turbine Cascade”, Journal of Turbomachinery, Vol 110, pp18-26, 1988.

[30] Zhou, C., Hodson, H., Tibbott, I., Stokes, M., “The Aero-thermal Performance of a Cooled Winglet Tip in A High Speed Turbine Cascade”, ASME paper, GT2011-46369, 2011